High-pressure synthesis and neutron scattering study of tantalum hydride $TaH_{1.23(5)}$ and a tantalum polymorph with A15-type structure

Mikhail A. Kuzovnikov,[1,*] Thomas Hansen,[2] Alexandre S. Ivanov,[2] Alexander I. Kolesnikov,[3] Valery I. Kulakov,[4] Stanislav Savvin,[2] and Marek Tkacz[5]

[1]*Centre for Science at Extreme Conditions and School of Physics and Astronomy, University of Edinburgh, Edinburgh EH9 3FD, United Kingdom*

[2]*Institut Laue-Langevin, 71 avenue des Martyrs CS 20156, 38042 Grenoble Cedex 9, France*

[3]*Neutron Scattering Division, Oak Ridge National Laboratory, Oak Ridge, Tennessee 37831, USA*

[4]*Institute of Solid State Physics RAS, 142432 Chernogolovka, Moscow District, Russia*

[5]*Institute of Physical Chemistry PAS, 44/52 Kasprzaka, 01-224 Warsaw, Poland*

(Received 2 April 2024; revised 19 September 2024; accepted 28 October 2024; published xxxxxxxxxx)

A unique type of tantalum hydride was synthesized by exposing tantalum dihydride to the high hydrogen pressure of 9 GPa and a temperature of 580 °C using toroid-type high-pressure chambers. The samples of this hydride were cooled down to 100 K, recovered to ambient pressure, and studied in a metastable state by hot extraction, powder x-ray and neutron diffraction, and inelastic neutron scattering. X-ray diffraction demonstrated that this hydride had an A15-type crystal structure of metal lattice (space group *Pm*-3*n*, Ta atoms at the 2*a* and 6*c* Wyckoff positions) and a lattice parameter of $a = 5.510(5)$ Å at $T = 85$ K. The hydrogen content determined by hot extraction was H/Ta = 1.23(5). Hydrogen desorption during heating the sample in vacuum proceeded in two steps—first, ΔH/Ta = 0.2 was desorbed at around −70 °C, and then the rest of the hydrogen was desorbed between 100 °C and 390 °C. The A15-type metal lattice was preserved upon hydrogen removal, leaving a unique polymorph of tantalum. Neutron diffraction of A15-$TaH_{1.23(5)}$ demonstrated that hydrogen atoms occupy the 24*k* and 16*i* Wyckoff sites in the crystal structure, and annealing at 250 K resulted in a decrease of the 24*k* and an increase of the 16*i* site occupancies. Inelastic neutron scattering revealed four vibrational modes in the fundamental band of A15-$TaH_{1.23(5)}$ at 72, 135, 145, and 166 meV, the first three and the last one of which were tentatively assigned to the vibrations of H atoms at the 24*k* and 16*i* sites, respectively. No superconductivity was found in A15-$TaH_{1.1}$ and hydrogen-free A15-Ta at temperatures down to 1.5 K.

DOI: 10.1103/PhysRevB.00.004100

I. INTRODUCTION

High pressure is a powerful tool for the synthesis of novel materials with unusual properties. This particularly applies to hydrides, because high pressure dramatically increases the Gibbs free energy of molecular hydrogen, increasing its reactivity. With the recent advances in the diamond anvil cell (DAC) technique, hydrogen pressures up to 100 GPa became routinely available in many laboratories worldwide, which resulted in the discovery of a series of hydrides with unusually high hydrogen content [1], many of which turned out to be high-temperature superconductors. Particularly, the superconductivity was observed at ∼100 K and 130 GPa in hexagonal close packed (hcp) CeH_9, at 115 K and 95 GPa in face centered cubic (fcc) CeH_{10} [2], at 146 K and 170 GPa in hcp-ThH_9, at 161 K and 170 GPa in fcc-ThH_{10} [3], at 203 K and 150 GPa in body centered cubic (bcc) H_3S [4], at ∼215 K and 172 GPa in bcc-CaH_6 [5], at ∼220 K and ∼170 GPa in bcc-YH_6 [6,7], at 243 K and 201 GPa in hcp-YH_9 [7], and at 250 K and 170 GPa in fcc-LaH_{10} [8,9].

The majority of recently discovered hydrides adopt either a bcc, hcp, or fcc metal lattice, or distorted variants of these. However, there are a limited number of hydrides that adopt a rare A15-type metal lattice, also known as β-W type. These include β-UH_3 [10], A15-CeH_3 [11], A15-$Ba_8H_{\sim 46}$ [12], A15-Eu_8H_{40-46} [13,14], A15-$Y_8H_{\sim 46}$ [15], and A15-$La_8H_{\sim 46}$ [16–18], first observed in [19], where it was incorrectly identified as "$C2/m$-LaH_n".

It should be noted that the experimental characterization of the compositions and full crystal structures of novel high-pressure hydrides produced with the DAC technique is extremely challenging due to the small sample mass. Except for hcp-$TaH_{2.2}$ [20,21], none of the hydrides discovered in the DACs have their compositions and full crystal structures firmly established. A common approach is to assign the compositions by comparing the $V(P)$ dependencies for new hydrides, measured experimentally, with the results of DFT-based *ab initio* calculations. In this way, uncontrollable uncertainties can be introduced, particularly, due to the

*Contact author: m.kuzovnikov@ed.ac.uk

inability of present-day calculations to take nonstoichiometry into account.

Presently, the following tantalum hydrides are known at room temperature. Below 2.2 GPa a series of complex phases with $0 \leqslant \mathrm{H/Ta} \leqslant 0.89$ exists with hydrogen atoms ordered at the tetrahedral interstitial sites of the slightly distorted bcc lattice of Ta atoms [22–24]. Between 2.2 and 42 GPa [20], an hcp-$TaH_{2.2}$ is stable, in which hydrogen atoms occupy tetrahedral and octahedral interstitials [21]. Previously, we studied the full crystal structure and the vibrational spectra of tetragonal t-$TaH_{0.89}$ [24] and hcp-$TaH_{2.2}$ [21] with neutron diffraction and inelastic neutron scattering. The equilibrium pressure of the t-$TaH_{0.89} + xH_2 =$ hcp-$TaH_{2.2}$ reaction increases with increasing temperature, reaching 7.7 GPa at 470 °C [25]. Above 42 GPa, $cI16$-TaH_3 [26] is stable up to at least 85 GPa, in which hydrogen atoms tentatively occupy tetrahedral interstitials in the distorted bcc lattice of Ta atoms. Recently, superconductivity with a $T_c = 30$ K was observed in $cI16$-TaH_3 at around 200 GPa [27].

In this work, we tried to extend the line of the t-$TaH_{0.89} + xH_2 =$ hcp-$TaH_{2.2}$ equilibrium to higher pressures and temperatures. Surprisingly, we found that heating hcp-$TaH_{2.2}$ at 9 GPa did not result in a direct conversion to t-$TaH_{0.89}$. Instead, a unique hydride was formed with the A15-type crystal structure of metal atoms and a composition of $\mathrm{H/Ta} = 1.23(5)$.

II. EXPERIMENTAL DETAILS

Plates of a 99.9% Ta foil with a thickness of 0.16 mm and a total weight of 150–200 mg were exposed to a hydrogen atmosphere in a toroid-type high-pressure chamber [28] at 9 GPa, which was the maximal achievable pressure, using NH_3BH_3 as an internal hydrogen source [29]. The amount of NH_3BH_3 was chosen to ensure that hydrogen was in excess during the experiment. We used a silver ampoule and a thin spacer of h-BN to avoid physical contact of the sample with the ampoule walls and hydrogen source. The sample was loaded with hydrogen at 150 °C for 24 h, then at 100 °C for 24 h. Our previous works [20,21], which describe the synthesis in more detail, showed that almost pure hcp-$TaH_{2.2}$ is formed as a result of such treatment. The temperature was then increased to a desired value between 500 °C and 600 °C and, after the sample was equilibrated for 14–17 min, it was rapidly cooled (quenched) together with the chamber to the liquid N_2 temperature, and the pressure was released. The chamber was disassembled at ambient pressure under liquid nitrogen; the sample was recovered from the chamber and further stored in liquid nitrogen in order to prevent hydrogen losses.

Each recovered sample was examined by x-ray diffraction with Cu $K\alpha$ radiation at $T = 85$ K in a home-designed nitrogen flow cryostat mounted on a Siemens D500 diffractometer equipped with a diffracted beam monochromator. The XRD patterns of the annealed samples were recorded at the same temperature, to separate the possible thermal expansion effect from the lattice contraction due to hydrogen loss. The obtained diffraction patterns were analyzed by the Rietveld profile refinements method using POWDERCELL 2.4 [30] software. A small piece of each sample (a few milligrams) was also analyzed with hot extraction by heating it at a rate of 10 °C/min in a calibrated preevacuated volume, as described elsewhere [31]. Prior to the neutron scattering experiments, the samples were ground in an agate mortar under liquid nitrogen to reduce texture effects.

One sample with a mass of about 80 mg, containing about 62 wt % A15-$TaH_{1.23}$ + 25 wt % hcp-$TaH_{2.2}$ + 13 wt % t-$TaH_{0.89}$ according to XRD, was studied by neutron diffraction with the high-luminosity D20 diffractometer at ILL, Grenoble [32,33], using a Ge(117) monochromator with vertical focusing in the high-resolution configuration. The monochromator takeoff angle of about 118° was used to select neutrons with a wavelength of 1.3582 Å, as determined from a Rietveld analysis of the diffraction pattern of a $Na_2Ca_3Al_2F_{14}$ standard measured separately. The sample was loaded into a cylinder made of thin aluminum foil, which was placed under liquid nitrogen into a standard vanadium holder with an inner diameter of 5 mm. Unwanted parts of the sample holder were masked with cadmium foil, which produced some sharp peaks at large angles of $2\theta > 140°$. The data acquisition time at $T = 100$ K was 20 h, after which the sample was warmed in a cryostat to 250 K for 10 min, and another pattern was collected at $T = 100$ K for 15 h. Rietveld refinements were done with the FULLPROF 7.00 program [34].

Another sample with a mass of 119 mg, containing about 61 wt % A15-$TaH_{1.23}$ + 25 wt % t-$TaH_{0.89}$ + 14 wt % hcp-$TaH_{2.2}$, according to XRD, was studied by inelastic neutron scattering (INS) with the IN1-Lagrange inverted geometry spectrometer [35] installed at the hot source of the high-flux reactor at the Institute Laue-Langevin in Grenoble [36]. The INS spectrum was collected at $T = 10$ K for 8 h, the sample was warmed to room temperature, exposed for 12 h, and another INS spectrum was collected at $T = 10$ K for 9 h. A background from the cryostat and sample holder, a contribution from ice, and the contributions from impurity phases t-$TaH_{0.89}$ [24] and hcp-$TaH_{2.2}$ [21] were measured separately under the same conditions and subtracted from the experimental INS spectra. More details on the neutron scattering experiments can be found elsewhere [21,24]. The resulting spectra were normalized to the neutron flux at the sample.

After exposing this sample at room temperature for 5 years it contained 55 wt % A15-$TaH_{0.95}$ + 45 wt % t-$TaH_{0.76}$ according to XRD. The dynamic structure factor $S(Q, E)$ of this sample was studied with inelastic neutron scattering using the Fine Resolution Fermi Chopper Spectrometer (SEQUOIA) [37,38] at the Spallation Neutron Source at Oak Ridge National Laboratory. To provide an energy resolution of 1%–5% over a wide range of energy transfers ($E < 600$ meV), the data were collected with the incident neutron energies of $E_i = 18$, 50, 210, and 600 meV. The measurements were performed at a temperature of 5 K using a bottom-loading closed cycle helium refrigerator. The background from the aluminum sample holder has been measured at the same conditions and subtracted from the data. The collected INS data were corrected for detector efficiency and transformed from the time of flight and instrument coordinates to the dynamic structure factor $S(Q, E)$ by using the MANTIDPLOT [39] and DAVE [40] software packages for data reduction and analysis.

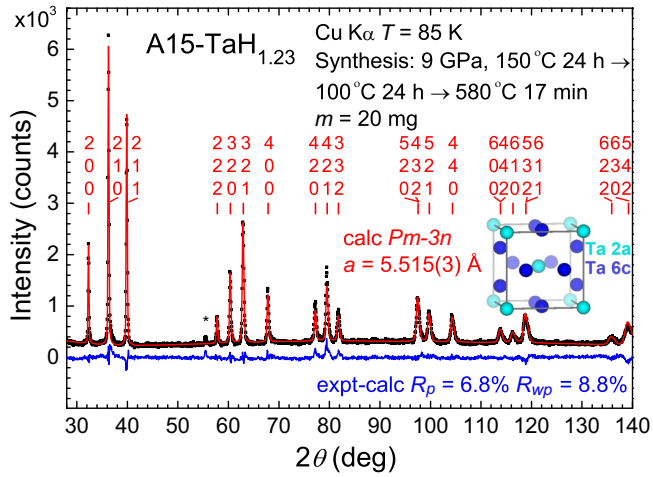

FIG. 1. Powder x-ray diffraction pattern of the Ta-H sample recovered after exposing hcp-$TaH_{2.2}$ to a hydrogen atmosphere at 9 GPa and $T = 580\,^{\circ}C$ for 17 min (black squares), the result of the Rietveld fit of the pattern with the A15 model of the crystal structure of a metal lattice (red curve), and the fit residual (blue curve). An impurity peak from hBN at 55.5° [29] is marked with an asterisk.

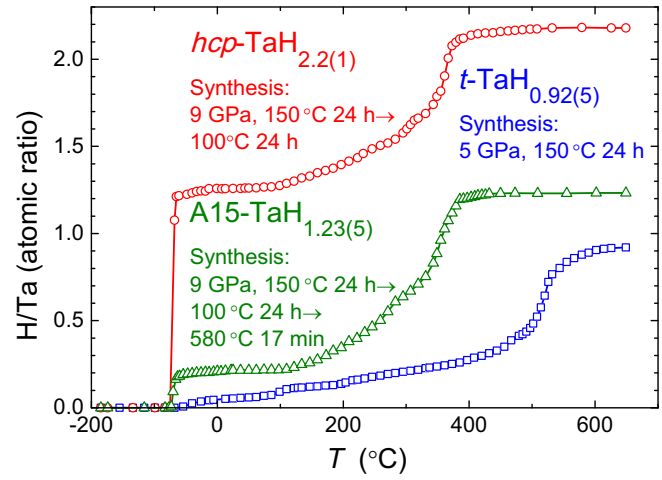

FIG. 2. Hydrogen desorption from A15-$TaH_{1.23}$ (green symbols and curve) upon heating the sample at a rate of 10 °C/min in a calibrated preevacuated volume. The desorption curves of hcp-$TaH_{2.2}$ (red) and t-$TaH_{0.92}$ (blue), studied previously in Ref. [20], are given for comparison.

III. RESULTS AND DISCUSSION

A. X-ray diffraction

Extrapolation of the experimental conditions for the reaction hcp-$TaH_{2.2} \rightarrow t$-$TaH_{0.89} + xH_2$ observed in Ref. [25] suggests that at 9 GPa, hcp-$TaH_{2.2}$ should decompose at about 580 °C. We performed a series of experiments, in which hcp-$TaH_{2.2}$ was first synthesized at 9 GPa using a previously established route [20,21] and then annealed at selected temperatures at the same pressure. In all annealing experiments at temperatures below 500 °C, the recovered product was hcp-$TaH_{2.2}$, and for temperatures above 620 °C the recovered product contained only t-$TaH_{0.89}$. However, an additional phase was present in the samples annealed between 500 °C and 620 °C, often in a mixture with t-$TaH_{0.89}$ and hcp-$TaH_{2.2}$. A typical x-ray powder diffraction pattern of a sample recovered after annealing at 580 °C for 17 min is shown in Fig. 1.

This new phase adopted an A15-type (also known as β-W-type) crystal structure of metal atoms, which occupied the $2a(0\,0\,0)$ and $6c(1/4\,0\,1/2)$ Wyckoff positions within the $Pm\text{-}3n$ space group (see inset in Fig. 1). Previously, no such phase was reported in any transition metal hydride. The lattice parameter of this new phase at ambient pressure and 85 K is $a = 5.510(5)$ Å (average of three syntheses).

Unlike the majority of the recovered high-pressure hydrides of transition metals, including hcp-$TaH_{2.2}$, which release most of the hydrogen and decompose upon warming to room temperature, the metal lattice in this A15 hydride proved to be remarkably (meta)stable. When this A15 hydride was warmed to room temperature and further to 300 °C, its lattice parameter measured at 85 K shrank to $a = 5.480(3)$ Å and 5.328(5) Å, respectively, indicating partial loss of hydrogen. No traces of decomposition back into t-TaH_{1-x} could be detected. The hydrogen release from the A15 sample stopped at approx. 390 °C. After annealing at 650 °C, the sample partially transformed into the original bcc crystal structure with $a = 3.303(5)$ Å, skipping the formation of t-TaH_{1-x} again. The lattice parameter of the hydrogen-free A15-Ta in the resulting two-phase mixture was $a = 5.281(5)$ Å at 85 K (Fig. SM1 in the Supplemental Material [41]; also see Ref. [42]), or $a = 5.295(5)$ Å at room temperature (RT).

Apart from stable bcc and metastable β-U-type [43] crystalline forms, A15-Ta represents the third crystalline form of tantalum. The existence of metastable A15-Ta with a small formation enthalpy of about H_{DFT}(A15-Ta) = 30 meV/Ta atom has been predicted by quantum chemistry calculations within density-functional theory (DFT) [44,45]. Apparently, such a small energy difference together with a large structural dissimilarity between stable bcc and metastable A15 polymorphs kinetically impedes a transformation of A15-Ta into original bcc crystal structure even at temperatures as high as 650 °C.

The situation when hydrogen desorption occurs before the transformation back into the stable crystalline form of an element is rare in binary hydrides. For example, recently an ω-$YH_{\sim 3}$ hydride was synthesized under high pressure of 45 GPa and a temperature of 3400 K [46]. Upon decompression at room temperature ω-$YH_{\sim 3}$ loses all of its hydrogen, but instead of converting back into hcp-Y (or one of the previously known yttrium hydrides), it leaves behind a unique yttrium polymorph, ω-Y.

B. Hot extraction

When heated in a vacuum, the recovered A15 phase desorbed hydrogen in two steps—first, ΔH/Ta ≈ 0.2 was desorbed at around −70 °C, and then ΔH/Ta ≈ 1.0 was desorbed in a broad temperature interval between 100 °C and 390 °C, as shown by the green curve in Fig. 2. The overall hydrogen content was H/Ta = 1.23(5). The shape of the desorption curve is similar to that of hcp-$TaH_{2.2}$, studied previously [20]; however, the magnitude of the first desorption

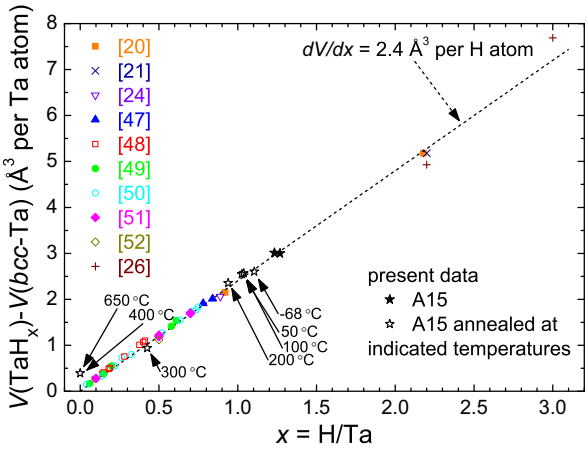

FIG. 3. Composition-volume relationship for currently known tantalum hydrides. The data of the present work for the "as-recovered" A15-$TaH_{1.23}$ are shown by filled stars, and the open stars stand for the A15 hydride annealed in vacuum at the indicated temperatures. The stars at $x = 0$ for the hydrogen-free A15 polymorph of tantalum are obtained for the samples annealed at 400 °C and 650 °C, and partially transformed into bcc-Ta. Other symbols show the literature data [20,21,24,26,47–52]. The solid line is a guide for the eye, indicating the hydrogen-induced volume expansion of the tantalum lattice by 2.4 Å^3 per H atom. The composition of *cI*16-TaH_3 [26], indicated by the rightmost down-triangle, is tentative.

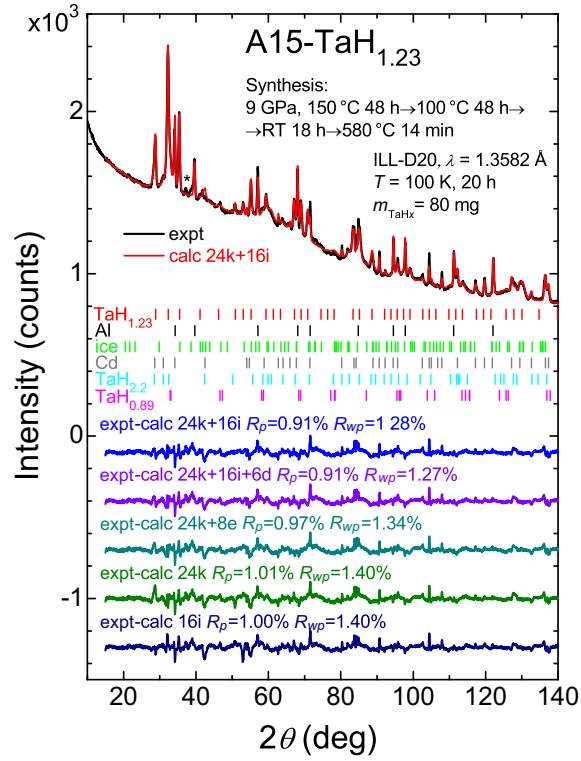

FIG. 4. Neutron powder diffraction pattern of the A15-$TaH_{1.23}$ sample (black curve) measured at $T = 100$ K with the D20 instrument at ILL, and the results of its Rietveld analysis using the structural model with hydrogen atoms occupying the 24*k* and 16*i* sites (red curve). The five bottom curves show the refinement residuals for this structural model (blue curve) and for alternative models, in which (i) hydrogen atoms additionally occupy 6*d* sites (violet), (ii) the adjacent 16*i* sites were merged to form a single 8*e* site (dark cyan), and (iii) hydrogen atoms were only allowed at the 24*k* (dark green) and 16*i* (dark blue) sites. The minor contributions from the aluminum sample capsule, ice, cadmium mask, and contaminant t-$TaH_{0.89}$ and hcp-$TaH_{2.2}$ phases were accounted for in Rietveld refinements using the same set of refinable parameters. The refined structural parameters for these model crystal structures of the main A15 phase are listed in Table I. The asterisk indicates the peak from the vanadium sample holder at 37°.

step is much smaller. Surprisingly, the first step of hydrogen desorption occurs at the same temperature of −70 °C in A15-$TaH_{1.23}$ and hcp-$TaH_{2.2}$, despite the differences in their crystal structures. In contrast to hcp-$TaH_{2.2}$, in which the first desorption step is associated with the conversion into t-TaH_{1-x}, the metal lattice of the A15 hydride is retained at this step, leaving A15-$TaH_{1.1}$ as a product.

To investigate the thermal stability of A15-TaH_x, we annealed this phase in vacuum at progressively increasing temperatures of −68 °C, 50 °C, 100 °C, 200 °C, 300 °C, 400 °C, and 650 °C. After each annealing we collected an XRD pattern at 85 K, chipped off a small part of the sample, and analyzed it by hot extraction at temperatures up to 650 °C. The resulting dependence of lattice volumes of the A15-TaH_x phase on its composition x is shown in Fig. 3 by filled and open stars in comparison with the $V(x)$ data for other presently known tantalum hydrides.

As can be seen from Fig. 3, this dependence follows a linear trend with $dV/dx = 2.4$ Å^3 per H atom, characteristic of all presently known tantalum hydrides (the V(H/Ta) data for presently known tantalum hydrides are also summarized in Table SM1 [41]). This value is typical of transition metals, in which hydrogen occupies tetrahedral interstitial sites [48–53].

The volume of hydrogen-free A15-Ta at 85 K is by 0.4(1) Å^3 per Ta atom larger than that of bcc-Ta at the same temperature, in agreement with recent DFT-based *ab initio* predictions of V_{DFT}(A15-Ta)-V_{DFT}(bcc-Ta) = 0.4 Å^3 per Ta atom [44] or 0.5 Å^3 per Ta atom [45]. For comparison, a well-known metastable beta (A15) modification of tungsten has V(A15-W) − V(bcc-W) = 0.1 Å^3 per W atom [54].

C. Neutron diffraction

The neutron powder diffraction pattern of this A15-$TaH_{1.23}$ hydride is shown in Fig. 4. Regretfully, the samples of the A15 phase synthesized for the neutron scattering studies were contaminated by both t-$TaH_{0.89}$ and hcp-$TaH_{2.2}$. Nevertheless, the quality of the diffraction pattern was sufficient to discriminate between possible model candidates for the full crystal structure of the A15 phase.

The A15-type structure features three interstitial sites, 24*k*, 16*i*, and 6*d*, all having tetrahedral coordination. In β-UH_3, which is the only binary hydride with the A15-type metal lattice known until recently, hydrogen atoms occupy 24*k* sites only [10]. DFT-based *ab initio* calculations suggested that A15-CeH_3, recently discovered in DACs, should be isomorphic to β-UH_3 [11]. In A15-$Ba_8H_{\sim 46}$ [12] and A15-$La_8H_{\sim 46}$ [17] *ab initio* calculations predicted full occupancy of all tetrahedral interstitials, which makes their crystal structure

TABLE I. Refined parameters of various structural models for A15-$TaH_{1.23}$. All refinements were carried out with the same set of refinable parameters, which included the profile functions, instrumental parameters, background, absorption correction, atomic coordinates, occupancies, and atomic displacement parameters. The refinement residuals for each model are shown at the bottom of Fig. 4. All model structures belong to the space group *Pm*-3*n* (No. 223), and their refined lattice parameter is $a = 5.5064(8)$ Å. In each model the atomic displacement parameters for all hydrogen atoms were assumed to be identical.

Model	Structure representation	Atom	Wyckoff position	*x*	*y*	*z*	*w*	U_{iso} (Å^2)	Shortest H–H distances (Å)	R_p (%)	R_{wp} (%)
24*k*+16*i*	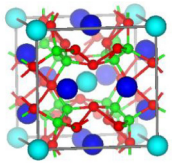	Ta1	2*a*	0	0	0	1	0.008(5)	H1–H1=1.61 H1–H2=1.30 H2–H2=0.93	0.91	1.28
		Ta2	6*c*	1/4	0	1/2	1	0.013(3)			
		H1	24*k*	0	0.175(10)	0.323(10)	0.19(5)	0.01(2)			
		H2	16*i*	0.201(5)	0.201(5)	0.201(5)	0.20(5)	0.01(2)			
24*k*+16*i*+6*d*	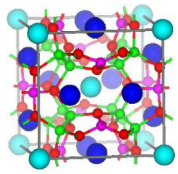	Ta1	2*a*	0	0	0	1	0.004(5)	H1–H1=1.63 H1–H2=1.29 H1–H3=1.07 H2–H2=0.98 H2–H3=2.01 H3–H3=2.75	0.91	1.27
		Ta2	6*c*	1/4	0	1/2	1	0.015(4)			
		H1	24*k*	0	0.174(10)	0.321(10)	0.18(5)	0.01(2)			
		H2	16*i*	0.198(7)	0.198(7)	0.198(7)	0.20(5)	0.01(2)			
		H3	6*d*	1/4	1/2	0	0.07(5)	0.01(2)			
24*k*+8*e*	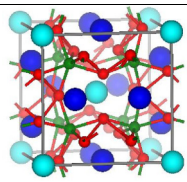	Ta1	2*a*	0	0	0	1	0.009(5)	H1–H1=1.65 H1–H2=1.49 H2–H2=2.75	0.97	1.34
		Ta2	6*c*	1/4	0	1/2	1	0.012(3)			
		H1	24*k*	0	0.172(10)	0.319(8)	0.28(8)	0.02(2)			
		H2	8*e*	1/4	1/4	1/4	0.24(8)	0.02(2)			
24*k*	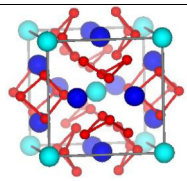	Ta1	2*a*	0	0	0	1	0.005(4)	H1–H1=1.65	1.01	1.40
		Ta2	6*c*	1/4	0	1/2	1	0.016(4)			
		H1	24*k*	0	0.182(8)	0.311(8)	0.25(8)	0.01(2)			
16*i*	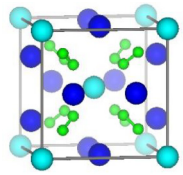	Ta1	2*a*	0	0	0	1	0.007(5)	H1–H1=0.96	1.00	1.40
		Ta2	6*c*	1/4	0	1/2	1	0.013(3)			
		H1	16*i*	0.200(5)	0.200(5)	0.200(5)	0.20(4)	–0.01(1)			

isomorphic to the well-known clathrate type I with hydrogen atoms as the "host" species. In A15-Eu_8H_{40-46}, some calculations predicted full occupancy of 24*k* and 16*i* sites and empty 6*d* sites [13], whereas other calculations predicted full occupancy of all tetrahedral interstitials [14]. Judging by the large divergence between the calculated and observed equations of state of A15-Eu_8H_{40-46} [14], a third possibility is realized—this phase, similar to many other hydrides, has a pressure-dependent nonstoichiometric composition with a fractional occupancy of 6*d* sites.

We fitted the experimental neutron powder diffraction pattern of A15-$TaH_{1.23}$ with the "24*k*" and "16*i*" structural models, in which hydrogen atoms were randomly distributed at 24*k* or 16*i* sites, respectively. It turned out that both models provide similar fit quality with residual *R* factors of $R_p = 1.00\%-1.01\%$ and $R_{wp} = 1.40\%$, as shown by the two bottom residual curves in Fig. 4. On the other hand, inclusion of both 24*k* and 16*i* sites in a "24*k* + 16*i*" model resulted in a significantly improved fit with $R_p = 0.91\%$ and $R_{wp} = 1.28\%$, as shown by the red and blue curves in Fig. 4. Thus this 24*k* + 16*i* model was adopted for the full crystal structure of A15-$TaH_{1.23}$.

As shown by the violet residual curve in Fig. 4, the inclusion of hydrogen atoms at the 6*d* sites did not improve the fit quality in the 24*k* + 16*i* + 6*d* model, which probably indicates the absence of hydrogen atoms at these sites.

The 16*i* sites form pairs with unusually short intersite distances *r*[H(16*i*)-H(16*i*)] ≈ 0.9 Å within each pair. We additionally analyzed a structural model in which the adjacent 16*i* sites were merged to form a single 8*e* site with planar triangular coordination. The residual factors for this 24*k* + 8*e* model, $R_p = 0.97\%$ and $R_{wp} = 1.34\%$, are somewhat worse than those of the original 24*k* + 16*i* model (see the dark cyan residual curve in Fig. 4), so we ruled out this model.

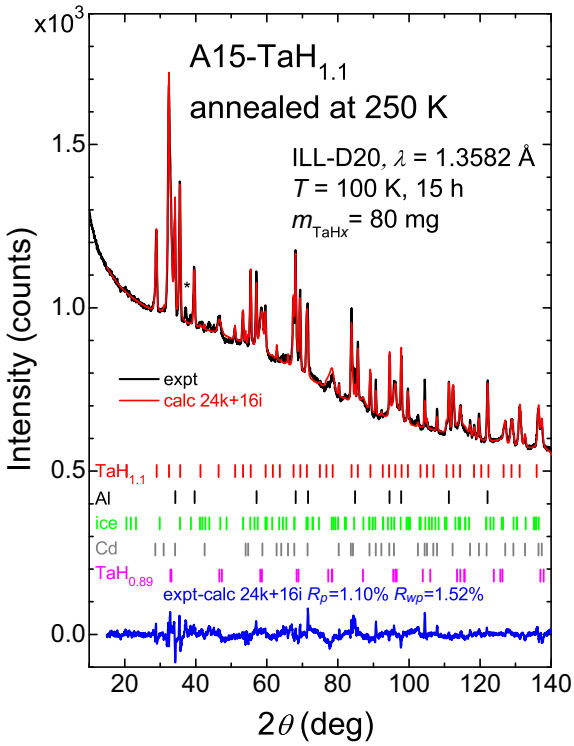

FIG. 5. Neutron powder diffraction pattern of the A15-$TaH_{1.1}$ sample annealed at 250 K and measured at 100 K with the D20 instrument at ILL (black curve). The results of the Rietveld refinement of the $24k + 16i$ structural model are shown by the red curve, and the blue curve is the refinement residual. The refined structural parameters of the main A15 phase are listed in Table II. The asterisk indicates the peak from the vanadium sample holder at 37°.

The refined structural parameters for all models are summarized in Table I. It must be noted that all models considered here have unusually small shortest H–H interatomic distances. Particularly, in the $24k + 16i$ model these are $r[\mathrm{H}(24k) - \mathrm{H}(24k)] = 1.61$ Å, $r[\mathrm{H}(24k) - \mathrm{H}(16i)] = 1.30$ Å, and $r[\mathrm{H}(16i) - \mathrm{H}(16i)] = 0.93$ Å. At the same time, the minimal distance between hydrogen atoms cannot be much less than 2 Å in any transition metal hydride, as suggested by Switendick [55]. There are a number of materials, such as $ZrCr_2D_{0.61}$ [56], $CaRh_2D_{3.20}$, and $CaRh_2D_{3.93}$ [57], in which the distance between crystallographic positions, partially occupied by hydrogen, is less than 2 Å. However, there are only two hydrides at ambient pressure—$LaNiInH(D)_{1.3}$ [58] and ZrV_2H_4 [59]—in which actual hydrogen atoms violate Switendick's criterion. For the $24k + 16i$ model of A15-$TaH_{1.23}$, the occupancies w of the $24k$ and $16i$ sites by hydrogen atoms converged to $w(24k) = 0.19(5)$ and $w(16i) = 0.20(5)$, which indicates that only a small fraction of interstitials is occupied by hydrogen atoms, so that the "2 Å" Switendick criterion could in principle be satisfied. If this is the case, anticorrelation in the occupancy of adjacent sites can result in a long-range ordering [24], and further neutron diffraction studies on deuterated samples are needed to explore this possibility.

The neutron powder diffraction pattern of the A15-$TaH_{1.1}$ sample after warming to 250 K is shown in Fig. 5. The warming resulted in the following changes. First, the hcp-$TaH_{2.2}$ impurity phase disappeared from the pattern due to its conversion into t-$TaH_{0.89}$. Second, the lattice parameter of the main A15 phase decreased from $a = 5.5064(8)$ Å to $a = 5.4827(4)$ Å, as shown in Table II. This corresponds to a change in composition from H/Ta = 1.23 to 1.1. Third, the results of the Rietveld refinement of the $24k + 16i$ crystal structure model, shown by the red and blue curves in Fig. 5, suggest that the occupancies of the $24k$ and $16i$ sites decreased to $w(24k) = 0.17(5)$ and increased to $w(16i) = 0.21(5)$, respectively; see Table II.

D. Inelastic neutron scattering

Neutron diffraction revealed that hydrogen atoms occupy closely spaced $16i$ and $24k$ sites in the crystal structure of A15-$TaH_{1.23}$ with $r(24k - 24k) = 1.61$ Å, $r(24k - 16i) = 1.30$ Å, and $r(16i - 16i) = 0.93$ Å, which violate the Switendick's 2 Å criterion [55]. However, neutron diffraction cannot tell if actual hydrogen atoms come closer than 2 Å to each other, because these sites are only partially occupied. To explore this possibility, we studied the vibrational dynamics of A15-TaH_x with inelastic neutron scattering.

Previously, the vibrational spectroscopy by INS was successfully used to demonstrate the existence of H–H pairs with r(H-H) ≈ 1.6 Å in $ZrV_2H_{3.7}$ [59] and $LaNiInH_{1.6}$ [60]. These pairs vibrate with a characteristic frequency of $E \approx 50$ meV, which falls in the gap between the lattice vibrations (typically, at $E < 30$ meV) and optical vibrations of isolated H atoms (typically, at $E > 90$ meV) and serves as a good indicator of the presence of such pairs.

Another possibility is realized in α-$MnH_{0.07}$, where one hydrogen atom occupies two positions with extremely short r(H–H) < 1 Å, which gives rise to a giant tunneling effect between these positions [61,62]. In α-$MnH_{0.07}$, an extremely strong tunneling mode at $E = 6.3$ meV has been observed in the INS spectrum.

TABLE II. Refined parameters of A15-$TaH_{1.1}$ after warming to 250 K. The refinement residual is shown at the bottom of Fig. 5. The space group is Pm-3n (No. 223), and the refined lattice parameter is $a = 5.4827(4)$ Å.

Model	Atom	Wyckoff position	x	y	z	w	U_{iso} (Å^2)	Shortest distances (Å)	R_p (%)	R_{wp} (%)
	Ta1	2a	0	0	0	1	0.012(4)	H1 − H1 = 1.57		
	Ta2	6c	1/4	0	1/2	1	0.012(2)	H1 − H2 = 1.36	1.10	1.52
$24k + 16i$	H1	24k	0	0.167(10)	0.335(10)	0.17(5)	0.02(2)	H2 − H2 = 0.76		
	H2	16i	0.210(5)	0.210(5)	0.210(5)	0.21(5)	0.02(2)			

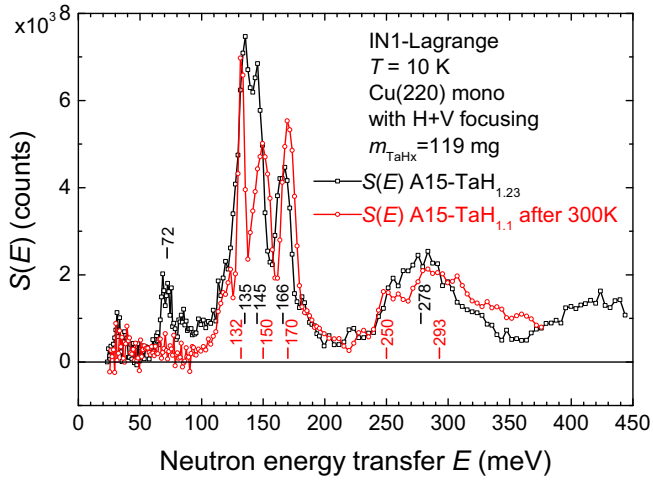

FIG. 6. The dynamical structure factors $S(E)$ of A15-$TaH_{1.23}$ (black curve) and A15-$TaH_{1.1}$ (red curve) collected with the IN1-Lagrange inelastic neutron scattering spectrometer, as a function of neutron energy loss E. The vertical ticks show the positions of the experimental peaks.

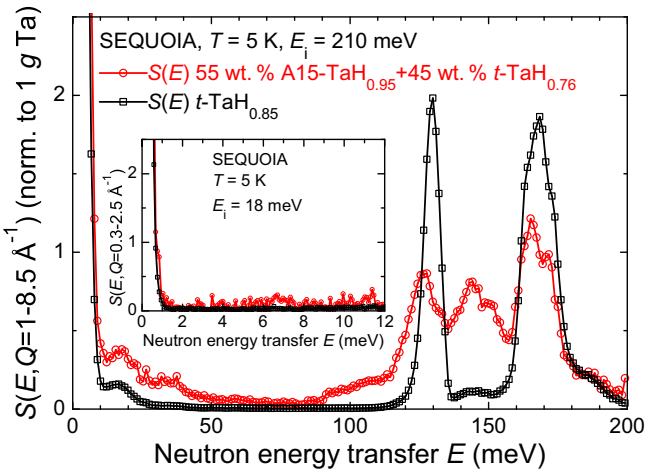

FIG. 7. INS spectra of A15-TaH_x (red) and t-TaH_x (black) measured at $T = 5$ K using the SEQUOIA spectrometer with $E_i = 210$ meV (main plot) and 18 meV (inset); the background from the sample holder has been subtracted from the data. The spectra are normalized to the neutron flux and sample masses. At $E \approx 0$ meV the spectra are dominated by the elastic line, and the excitations at 10 meV $< E <$ 25 meV are due to the lattice vibrations of tantalum atoms.

The INS spectrum of A15-$TaH_{1.23}$, collected with the IN1-Lagrange spectrometer at $T = 10$ K, is shown by the black curve in Fig. 6. The background from the cryostat, aluminum sample holder, and ice, condensed onto the sample surface during handling in liquid nitrogen, was subtracted, and the spectrum was normalized to the neutron flux. The INS spectra of the impurity phases t-$TaH_{0.89}$ [24] and hcp-$TaH_{2.2}$ [21], collected earlier with the same configuration of the spectrometer, were normalized to the amount of these phases measured by XRD and subtracted from the experimental spectrum of the A15-$TaH_{1.23}$ sample.

The fundamental vibrational band of hydrogen in A15-$TaH_{1.23}$ consists of four peaks at $E = 72$, 135, 145, and 166 meV. Spurious intensity below 60 meV results from minor contamination of the incoming neutron beam with $\lambda/2$ neutrons [63]. The broad feature centered at $E = 278$ meV apparently originates from two-phonon scattering.

The minor feature at $E = 72$ meV could result from the vibrations of H–H pairs with short interatomic distances of r(H-H) $\approx 1.6 - 1.7$ Å. However, we cannot completely exclude that this feature could be an artifact resulting from the undersubtraction of ice admixture, which has a step-like intensity increase at $E > 67$ meV, and oversubtraction of hcp-$TaH_{2.2}$ impurity, which has a sharp peak at $E = 80$ meV [21]. Further studies on pure A15-TaH_{1+x} samples are required to exclude this possibility.

After annealing at room temperature, the A15-$TaH_{1.1}$ sample was cooled to $T = 10$ K, and its INS spectrum was collected, as shown by the red curve in Fig. 6. The background from the cryostat, aluminum sample holder, and impurity phase t-$TaH_{0.89}$ [24] was subtracted, and the spectrum was normalized to the same neutron flux as that of A15-$TaH_{1.23}$. No subtraction of ice and hcp-$TaH_{2.2}$ admixtures was performed in this case, because these phases disappeared during the room-temperature annealing.

Annealing at room temperature resulted in a disappearance of the feature at $E = 72$ meV and a shift of the fundamental vibration features to $E = 132$, 150, and 170 meV. The intensities of the first two features decreased, while the intensity of the 170 meV feature increased. One could speculate that the observed intensity redistribution is related to the redistribution of hydrogen atoms between the 24k and 16i interstitial sites, as discussed in the previous section. In this case, the features at $E = 72$, 135, and 145 meV can be attributed to the vibrations of hydrogen atoms at the 24k sites, and the feature at $E = 166$ meV can be associated with vibrations of hydrogen atoms at the 16i sites.

In order to explore the low-energy part of the dynamical structure factor $S(Q, E)$, this sample was studied with inelastic neutron scattering using the SEQUOIA spectrometer at ORNL. By that time, the sample had been exposed to room temperature for 5 years and lost some of its hydrogen, containing a mixture of 55 wt % A15-$TaH_{0.95}$ + 45 wt % t-$TaH_{0.76}$ according to XRD. The resulting contour plots for $S(Q, E)$ for this sample in comparison to that of pure t-$TaH_{0.85}$ are presented in Fig. SM2 [41], and the $S(E)$ spectra for $E_i = 210$ meV, obtained via integration over the whole Q range of $1 - 8.5$ Å^{-1} are shown in Fig. 7 by the red and black curves, respectively.

Comparing to t-$TaH_{0.85}$, in A15-$TaH_{0.95}$ we observe a continuum of low-energy excitations below 40 meV, and a hump in the frequency range between 90 and 115 meV. The latter could have the same origin as the 72 meV peak in the as-quenched A15-$TaH_{1.23}$, that is, the vibrations of short-spaced $24k - 24k$ or $24k - 16i$ pairs.

At the same time, we do not observe any well-defined tunneling mode between the short-spaced pairs of 16i sites analogous to the tunneling mode of hydrogen in α-$MnH_{0.07}$ [61,62]. In contrast to α-$MnH_{0.07}$, where the H–H interaction is negligible due to the low H/Me content, in A15-$TaH_{\sim 1}$ the nearby hydrogen atoms can perturb the potential well for

H atoms sitting at the 16*i* sites, making one of these sites more energetically preferable. Induced asymmetry between the 16*i* sites in the pair would likely result in an increase of the tunneling frequency, as well as in its smearing due to random occupancies of nearby sites. In order to test if the low-energy excitations below 40 meV in A15-TaH_x could be rationalized in this way, it would be desirable to study the INS on a deuterated A15-TaD_x counterpart in the future, because of extreme sensitivity of the tunneling mode frequency to the isotope mass [61].

E. Magnetic susceptibility

To explore possible superconductivity in A15-TaH_{1+x}, we measured the ac magnetic susceptibility of the annealed A15-$TaH_{1.1}$ sample at temperatures down to 1.5 K, using a homemade ac susceptometer. The sample was placed inside one of the two identical pickup coils positioned inside a long vertical excitation coil that provided a uniform ac drive magnetic field with an amplitude of a few oersteds and a frequency of 100 kHz. The signal was collected with an SR830 lock-in amplifier. We found no anomalies that could be associated with superconductivity.

Hydrogen was then removed from the sample by vacuum annealing at 400 °C for 30 min, which converted the sample into a mixture of bcc-Ta and A15-Ta in approximately equal amounts as evidenced by XRD. Apart from the superconducting transition at 4.4 K due to the bcc-Ta impurity, ac magnetic suspectometry did not reveal any transitions down to 1.5 K which could be associated with the superconductivity in A15-Ta.

IV. CONCLUSIONS

Massive powder samples of a unique tantalum hydride $TaH_{1.23(5)}$ were synthesized under high pressures and elevated temperatures and studied by hot extraction, x-ray diffraction, neutron diffraction, and inelastic neutron scattering in a metastable state at ambient pressure and low temperature. The metal lattice of this hydride has an A15-type cubic crystal structure, also known as β-W type, with a lattice parameter $a = 5.510(5)$ Å at $T = 85$ K and Ta atoms occupying 2*a* and 6*c* Wyckoff positions within the space group *Pm*-3*n*. According to the hot extraction analysis, hydrogen desorption upon heating proceeds in two stages: first, $\Delta H/Ta \approx 0.2$ is desorbed stepwise at $T \approx -70$ °C, and the remaining hydrogen is released in a wide temperature interval of 100 °C − 390 °C. Surprisingly, the A15 crystal structure of the metal lattice is retained in the hydrogen-free sample heated above 390 °C and only partially converts back to the original bcc structure at temperatures 400 °C − 650 °C. That is, the removal of hydrogen from A15-$TaH_{1.23(5)}$ by heating it in a vacuum to 400 °C − 650 °C produces a previously unknown bulk polymorph of tantalum with an A15-type crystal structure and lattice parameter $a = 5.281(5)$ Å at $T = 85$ K [$a = 5.295(5)$ Å at $T = 293$ K].

The neutron diffraction study of A15-$TaH_{1.23}$ demonstrated that hydrogen atoms occupy 24*k* and 16*i* interstitial sites in the tantalum lattice with fractional occupancies $w(24k) = 0.19(5)$ and $w(16i) = 0.20(5)$. Warming the sample to 300 K resulted in a partial loss of hydrogen from the 24*k* sites and a redistribution between the 24*k* and 16*i* sites.

The inelastic neutron scattering study of A15-$TaH_{1.23}$ revealed four features in the fundamental band of hydrogen vibrations at 72, 135, 145, and 166 meV, the first three of which were tentatively assigned to the vibrations of hydrogen atoms at the 24*k* sites, whereas the last one likely results from the hydrogen atoms at the 16*i* sites.

No superconductivity was found in A15-$TaH_{1.1}$ and hydrogen-free A15-Ta at temperatures down to 1.5 K.

ACKNOWLEDGMENTS

The research was supported by the Russian Science Foundation (Grant No. 23-22-00361). This result is part of a project that has received funding from the European Research Council (ERC) under the European Union's Horizon 2020 research and innovation program (Grant No. 948895, MetElOne). A portion of this research used resources at the Spallation Neutron Source, a U.S. DOE Office of Science User Facility operated by the Oak Ridge National Laboratory. The beam time was allocated to the SEQUOIA spectrometer by Proposal No. IPTS-33526.1. We would like to acknowledge Vladimir Zverev (ISSP RAS) for the susceptibility measurements, Vladimir Antonov (ISSP RAS), and Rebecca Rae (University of Edinburgh) for the x-ray diffraction measurements, and Mengnan Wang (Stanford University) for sample transportation.

[1] M. A. Kuzovnikov, V. S. Minkov, S. Chariton, V. B. Prakapenka, and M. I. Eremets, Synthesis of osmium hydride under high hydrogen pressure, Phys. Rev. B **102**, 214109 (2020).

[2] W. Chen, D. V. Semenok, X. Huang, H. Shu, X. Li, D. Duan, T. Cui, and A. R. Oganov, High-temperature superconducting phases in cerium superhydride with a T_c up to 115 K below a pressure of 1 megabar, Phys. Rev. Lett. **127**, 117001 (2021).

[3] D. V. Semenok, A. G. Kvashnin, A. G. Ivanova, V. Svitlyk, V. Yu. Fominski, A. V. Sadakov, O. A. Sobolevskiy, V. M. Pudalov, I. A. Troyan, and A. R. Oganov, Superconductivity at 161 K in thorium hydride ThH_{10}: Synthesis and properties, Mater. Today **33** (Mar), 36 (2020).

[4] A. P. Drozdov, M. I. Eremets, I. A. Troyan, V. Ksenofontov, and S. I. Shylin, Conventional superconductivity at 203 kelvin at high pressures in the sulfur hydride system, Nature (London) **525**, 73 (2015).

[5] L. Ma, K. Wang, Y. Xie, X. Yang, Y. Wang, M. Zhou, H. Liu, X. Yu, Y. Zhao, H. Wang, G. Liu, and Y. Ma, High-temperature superconducting phase in clathrate calcium hydride CaH_6 up to 215 K at a pressure of 172 GPa, Phys. Rev. Lett. **128**, 167001 (2022).

[6] I. A. Troyan, D. V. Semenok, A. G. Kvashnin, A. V. Sadakov, O. A. Sobolevskiy, V. M. Pudalov, A. G. Ivanova, V. B. Prakapenka, E. Greenberg, A. G. Gavriliuk, I. S. Lyubutin, V. V. Struzhkin, A. Bergara, I. Errea, R. Bianco, M. Calandra, F. Mauri, L. Monacelli, R. Akashi, and A. R. Oganov, Anomalous high-temperature superconductivity in YH_6, Adv. Mater. **33**, 2006832 (2021).

[7] P. Kong, V. S. Minkov, M. A. Kuzovnikov, A. P. Drozdov, S. P. Besedin, S. Mozaffari, L. Balicas, F. F. Balakirev, V. B. Prakapenka, S. Chariton, D. A. Knyazev, E. Greenberg, and M. I. Eremets, Superconductivity up to 243 K in the yttrium-hydrogen system under high pressure, Nat. Commun. **12**, 5075 (2021).

[8] A. P. Drozdov, P. P. Kong, V. S. Minkov, S. P. Besedin, M. A. Kuzovnikov, S. Mozaffari, L. Balicas, F. Balakirev, D. Graf, V. B. Prakapenka, E. Greenberg, D. A. Knyazev, M. Tkacz, and M. I. Eremets, Superconductivity at 250 K in lanthanum hydride under high pressures, Nature (London) **569**, 528 (2019).

[9] M. Somayazulu, M. Ahart, A. K. Mishra, Z. M. Geballe, M. Baldini, Y. Meng, V. V. Struzhkin, and R. J. Hemley, Evidence for superconductivity above 260 K in lanthanum superhydride at megabar pressures, Phys. Rev. Lett. **122**, 027001 (2019).

[10] W. Bartscher, A. Boeuf, R. Caciuffo, J. M. Fournier, W. F. Kuhs, J. Rebizant, and F. Rustichelli, Neutron diffraction study of β-UD_3 and β-UH_3, Solid State Commun. **53**, 423 (1985).

[11] N. P. Salke, M. M. D. Esfahani, Y. Zhang, I. A. Kruglov, J. Zhou, Y. Wang, E. Greenberg, V. B. Prakapenka, J. Liu, A. R. Oganov, and J.-F. Lin, Synthesis of clathrate cerium superhydride CeH_9 at 80–100 GPa with atomic hydrogen sublattice, Nat. Commun. **10**, 4453 (2019).

[12] M. Peña-Alvarez, J. Binns, M. Martinez-Canales, B. Monserrat, G. J. Ackland, P. Dalladay-Simpson, R. T. Howie, C. J. Pickard, and E. Gregoryanz, Synthesis of Weaire–Phelan barium polyhydride, J. Phys. Chem. Lett. **12**, 4910 (2021).

[13] L. Ma, M. Zhou, Y. Wang, S. Kawaguchi, Y. Ohishi, F. Peng, H. Liu, G. Liu, H. Wang, and Y. Ma, Experimental clathrate superhydrides EuH_6 and EuH_9 at extreme pressure conditions, Phys. Rev. Res. **3**, 043107 (2021).

[14] D. V. Semenok, D. Zhou, A. G. Kvashnin, X. Huang, M. Galasso, I. A. Kruglov, A. G. Ivanova, A. G. Gavriliuk, W. Chen, N. V. Tkachenko, A. I. Boldyrev, I. Troyan, A. R. Oganov, and T. Cui, Novel strongly correlated europium superhydrides, J. Phys. Chem. Lett. **12**, 32 (2021).

[15] A. Aslandukova, A. Aslandukov, D. Laniel, Y. Yin, F. I. Akbar, M. Bykov, T. Fedotenko, K. Glazyrin, A. Pakhomova, G. Garbarino, E. L. Bright, J. Wright, M. Hanfland, S. Chariton, V. Prakapenka, N. Dubrovinskaia, and L. Dubrovinsky, Diverse high-pressure chemistry in Y-NH_3BH_3 and Y–paraffin oil systems, Sci. Adv. **10**, eadl5416 (2024).

[16] D. Laniel, F. Trybel, B. Winkler, F. Knoop, T. Fedotenko, S. Khandarkhaeva, A. Aslandukova, T. Meier, S. Chariton, K. Glazyrin, V. Milman, V. Prakapenka, I. A. Abrikosov, L. Dubrovinsky, and N. Dubrovinskaia, High-pressure synthesis of seven lanthanum hydrides with a significant variability of hydrogen content, Nat. Commun. **13**, 6987 (2022).

[17] J. Guo, D. Semenok, G. Shutov, D. Zhou, S. Chen, Y. Wang, K. Zhang, X. Wu, S. Luther, T. Helm, X. Huang, and T. Cui, Unusual metallic state in superconducting A15-type La_4H_{23}, Natl. Sci. Rev. **11**, nwae149 (2024).

[18] S. Cross, J. Buhot, A. Brooks, W. Thomas, A. Kleppe, O. Lord, and S. Friedemann, High-temperature superconductivity in La_4H_{23} below 100 GPa, Phys. Rev. B **109**, L020503 (2024).

[19] Z. M. Geballe, H. Liu, A. K. Mishra, M. Ahart, M. Somayazulu, Y. Meng, M. Baldini, and R. J. Hemley, Synthesis and stability of lanthanum superhydrides, Angew. Chem., Int. Ed. **57**, 688 (2018).

[20] M. A. Kuzovnikov, M. Tkacz, H. Meng, D. I. Kapustin, and V. I. Kulakov, High-pressure synthesis of tantalum dihydride, Phys. Rev. B **96**, 134120 (2017).

[21] M. A. Kuzovnikov, V. E. Antonov, A. S. Ivanov, T. Hansen, S. Savvin, V. I. Kulakov, M. Tkacz, A. I. Kolesnikov, and V. M. Gurev, Neutron scattering study of tantalum dihydride, Phys. Rev. B **102**, 024113 (2020).

[22] A. San-Martin and F. D. Manchester, The H-Ta (hydrogen-tantalum) system, J. Phase Equilib. **12**, 332 (1991).

[23] T. Schober, Vanadium-, niobium- and tantalum-hydrogen, Solid State Phenom. **49–50**, 357 (1996).

[24] M. A. Kuzovnikov, V. E. Antonov, A. S. Ivanov, T. Hansen, S. Savvin, V. I. Kulakov, M. Tkacz, and A. I. Kolesnikov, Neutron scattering study of tantalum monohydride and monodeuteride, Int. J. Hydrogen Energy **46**, 20630 (2021).

[25] H. Saitoh, S. Takagi, T. Sato, and S.-i. Orimo, Pressure–temperature phase diagram of Ta-H system up to 9 GPa and 600 °C, Appl. Sci. **11**, 6719 (2021).

[26] J. Ying, X. Li, E. Greenberg, V. B. Prakapenka, H. Liu, and V. V. Struzhkin, Synthesis and stability of tantalum hydride at high pressures, Phys. Rev. B **99**, 224504 (2019).

[27] X. He, C. L. Zhang, Z. W. Li, S. J. Zhang, B. S. Min, J. Zhang, K. Lu, J. F. Zhao, L. C. Shi, Y. Peng *et al.*, Superconductivity observed in tantalum polyhydride at high pressure, Chin. Phys. Lett. **40**, 057404 (2023).

[28] L. G. Khvostantsev, V. N. Slesarev, and V. V. Brazhkin, Toroid type high-pressure device: History and prospects, High Pressure Res. **24**, 371 (2004).

[29] V. E. Antonov, B. M. Bulychev, V. K. Fedotov, D. I. Kapustin, V. I. Kulakov, and I. A. Sholin, NH_3BH_3 as an internal hydrogen source for high pressure experiments, Int. J. Hydrogen Energy **42**, 22454 (2017).

[30] W. Kraus and G. Nolze, POWDER CELL—a program for the representation and manipulation of crystal structures and calculation of the resulting x-ray powder patterns, J. Appl. Crystallogr. **29**, 301 (1996).

[31] I. O. Bashkin, V. E. Antonov, A. V. Bazhenov, I. K. Bdikin, D. N. Borisenko, E. P. Krinichnaya, A. P. Moravsky, A. I. Harkunov, Y. M. Shul'ga, Y. A. Ossipyan, and E. G. Ponyatovsky, Thermally stable hydrogen compounds obtained under high pressure on the basis of carbon nanotubes and nanofibers, JETP Lett. **79**, 226 (2004).

[32] T. C. Hansen, P. F. Henry, H. E. Fischer, J. Torregrossa, and P. Convert, The D20 instrument at the ILL: A versatile high-intensity two-axis neutron diffractometer, Meas. Sci. Technol. **19**, 034001 (2008).

[33] M. Kuzovnikov, A. Ivanov, S. Savvin, and M. Tkacz, Crystal structure of novel tantalum hydrides, Institut Laue-Langevin (ILL) (2019).

[34] J. Rodríguez-Carvajal, Recent advances in magnetic structure determination by neutron powder diffraction, Phys. B (Amsterdam) **192**, 55 (1993).

[35] A. Ivanov, M. Jiménez-Ruiz, and J. Kulda, IN1-LAGRANGE—the new ILL instrument to explore vibration dynamics of complex materials, J. Phys.: Conf. Ser. **554**, 012001 (2014).

[36] M. Kuzovnikov, A. Ivanov, and M. Tkacz, Vibrational dynamics of novel tantalum hydrides, Institut Laue-Langevin (ILL) (2019), https://doi.org/10.5291/ILL-DATA.7-01-487.

[37] M. B. Stone, J. L. Niedziela, D. L. Abernathy, L. DeBeer-Schmitt, G. Ehlers, O. Garlea, G. E. Granroth, M. Graves-Brook, A. I. Kolesnikov, A. Podlesnyak, and B. Winn, A comparison of four direct geometry time-of-flight spectrometers at the Spallation Neutron Source, Rev. Sci. Instrum. **85**, 045113 (2014).

[38] G. E. Granroth, A. I. Kolesnikov, T. E. Sherline, J. P. Clancy, K. A. Ross, J. P. C. Ruff, B. D. Gaulin, and S. E. Nagler, SEQUOIA: A newly operating chopper spectrometer at the SNS, J. Phys.: Conf. Ser. **251**, 012058 (2010).

[39] O. Arnold, J. C. Bilheux, J. M. Borreguero, A. Buts, S. I. Campbell, L. Chapon, M. Doucet, N. Draper, R. Ferraz Leal *et al.*, MANTID—Data analysis and visualization package for neutron scattering and μSR experiments, Nucl. Instrum. Methods Phys. Res., Sect. A **764**, 156 (2014).

[40] R. T. Azuah, L. R. Kneller, Y. Qiu, P. L. W. Tregenna-Piggott, C. M. Brown, J. R. D. Copley, and R. M. Dimeo, DAVE: A comprehensive software suite for the reduction, visualization, and analysis of low energy neutron spectroscopic data, J. Res. Natl. Inst. Stand. Technol. **114**, 341 (2009).

[41] See Supplemental Material at http://link.aps.org/supplemental/10.1103/PhysRevB.xx.xxxxxx for the experimental data. The Supplemental Material also contains Ref. [42].

[42] J. W. Arblaster, *Selected Values of the Crystallographic Properties of the Elements* (ASM International, Materials Park, OH, 2018), pp. 524–532.

[43] P. T. Moseley and C. J. Seabrook, The crystal structure of β-tantalum, Acta Crystallogr., Sect. B **29**, 1170 (1973).

[44] Y. Yao and D. D. Klug, Stable structures of tantalum at high temperature and high pressure, Phys. Rev. B **88**, 054102 (2013).

[45] N. Jakse, O. Le Bacq, and A. Pasturel, Prediction of the local structure of liquid and supercooled tantalum, Phys. Rev. B **70**, 174203 (2004).

[46] A. Aslandukova, A. Aslandukov, D. Laniel, S. Khandarkhaeva, G. Steinle-Neumann, T. Fedotenko, S. V. Ovsyannikov, Y. Yin, F. I. Akbar, K. Glazyrin *et al.*, High-pressure *hP*3 yttrium allotrope with $CaHg_2$-type structure as a prototype of the *hP*3 rare-earth hydride series, Phys. Rev. B **107**, 014103 (2023).

[47] A. W. Szafrański, M. Tkacz, S. Majchrzak, and H. Züchner, Resistometric studies of the Ta-H system at high pressures and low temperatures, J. Less Common Met. **101**, 523 (1984).

[48] H. Peisl, in *Hydrogen in Metals I*, edited by G. Alefeld and J. Völkl (Springer, Berlin, 1978), pp. 53–74.

[49] F. Ducastelle, R. Caudron, and P. Costa, Etude du systeme tantale-hydrogene: Diagramme d'equilibre et structure electronique, J. Phys. Chem. Solids **31**, 1247 (1970).

[50] B. Stalinski, X-ray analysis and magnetic susceptibilities of tantalum hydrides, Bull. Acad. Pol. Sci., Cl. 3 **2**, 245 (1954).

[51] R. Yamada, N. Watanabe, K. Sato, H. Asano, and M. Hirabayashi, Localized modes in tantalum hydrides studied by neutron inelastic scattering, J. Phys. Soc. Jpn. **41**, 85 (1976).

[52] H. Asano, Y. Ishikawa, and M. Hirabayashi, Single-crystal x-ray diffraction study on the hydrogen ordering in Ta_2H, J. Appl. Crystallogr. **11**, 681 (1978).

[53] Y. Fukai, *The Metal-Hydrogen System*, 2nd ed. (Springer-Verlag, Berlin, 2005).

[54] T. Millner, A. J. Hegediis, K. Sasvari, and J. Neugebauer, Über die bildungsbedingungen und eigenschaften des β-wolframs. Weiterer beitrag zur reduktion des wolframtrioxyds, Z. Anorg. Allg. Chem. **289**, 288 (1957).

[55] A. C. Switendick, Electronic structure of transition metal hydrides, in *Transition Metal Hydrides*, edited by R. Bau, Advances in Chemistry Series Vol. 167 (ACS, Washington, DC, 1978), pp. 264–282.

[56] H. Kohlmann, F. Fauth, P. Fischer, A. V. Skripov, V. N. Kozhanov, and K. Yvon, Low-temperature deuterium ordering in the cubic Laves phase derivative α-$ZrCr_2D_{0.66}$, J. Alloys Compd. **327**, L4 (2001).

[57] A. Götze, J. Möllmer, and H. Kohlmann, From the Laves phase $CaRh_2$ to the perovskite $CaRhH_3$-*in situ* investigation of hydrogenation intermediates $CaRh_2H_x$, Inorg. Chem. **57**, 10925 (2018).

[58] V. A. Yartys, R. V. Denys, B. C. Hauback, H. Fjellvag, I. I. Bulyk, A. B. Riabov, and Ya. M. Kalychak, Short hydrogen–hydrogen separations in novel intermetallic hydrides, $RE_3Ni_3In_3D_4$ (RE = La, Ce and Nd), J. Alloys Compd. **330**, 132 (2002).

[59] A. Borgschulte, J. Terreni, E. Billeter, L. Daemen, Y. Cheng, A. Pandey, Z. Łodziana, R. J. Hemley, and A. J. Ramirez-Cuesta, Inelastic neutron scattering evidence for anomalous H–H distances in metal hydrides, Proc. Natl. Acad. Sci. USA **117**, 4021 (2020).

[60] R. A. Klein, R. Balderas-Xicohténcatl, J. P. Maehlen, T. J. Udovic, C. M. Brown, R. Delaplane, Y. Cheng, R. V. Denys, A. J. Ramirez-Cuesta, and V. A. Yartys, Neutron vibrational spectroscopic evidence for short H···H contacts in the RNiInH$_{1.4;1.6}$ (R = Ce, La) metal hydride, J. Alloys Compd. **894**, 162381 (2022).

[61] V. E. Antonov, B. Dorner, V. K. Fedotov, G. Grosse, A. S. Ivanov, A. I. Kolesnikov, V. V. Sikolenko, and F. E. Wagner, Giant tunnelling effect of hydrogen and deuterium in α manganese, J. Alloys Compds **330**, 462 (2002).

[62] A. I. Kolesnikov, A. Podlesnyak, R. A. Sadykov, V. E. Antonov, M. A. Kuzovnikov, G. Ehlers, and G. E. Granroth, Pressure effect on hydrogen tunneling and vibrational spectrum in α-Mn, Phys. Rev. B **94**, 134301 (2016).

[63] V. E. Antonov, A. I. Beskrovnyy, V. K. Fedotov, A. S. Ivanov, S. S. Khasanov, A. I. Kolesnikov, M. K. Sakharov, I. L. Sashin, and M. Tkacz, Crystal structure and lattice dynamics of chromium hydrides, J. Alloys Compd. **430**, 22 (2007).